Published in final edited form as:
Nat Commun. 2010 July 13; 1(4): . doi:10.1038/ncomms1037.

PI(3,5)P_2 Controls Membrane Traffic by Direct Activation of Mucolipin Ca^{2+} Release Channels in the Endolysosome

Xian-ping Dong[1,#], **Dongbiao Shen**[1,#], **Xiang Wang**[1,#], **Taylor Dawson**[1], **Xinran Li**[1], **Qi Zhang**[1], **Xiping Cheng**[1], **Yanling Zhang**[2], **Lois S. Weisman**[2], **Markus Delling**[3], and **Haoxing Xu**[1,*]

[1]The Department of Molecular, Cellular, and Developmental Biology, the University of Michigan, 3089 National Science Building (Kraus), 830 North University, Ann Arbor, MI 48109, USA

[2]The Department of Cell and Developmental Biology and Life Sciences Institute, University of Michigan, Ann Arbor, MI 48109-2216, USA

[3]The Department of Cardiology, Children's Hospital Boston, Enders 1350, 320 Longwood Avenue, Boston, MA 02115, USA

Abstract

Membrane fusion and fission in intracellular trafficking is controlled by both intraluminal Ca^{2+} release and phosphoinositide signaling. However, the molecular identities of the Ca^{2+} release channels and the target proteins of phosphoinositides are elusive. Here, by direct patch-clamping of the endolysosomal membrane, we report that PI(3,5)P_2, an endolysosome-specific phosphoinositide, binds and activates endolysosome-localized mucolipin TRP (TRPML) channels with specificity and potency. Both PI(3,5)P_2-deficient cells and cells that lack TRPML1 exhibited enlarged endolysosomes/vacuoles and trafficking defects in the late endocytic pathway. We find that the enlarged vacuole phenotype observed in PI(3,5)P_2-deficient mouse fibroblasts is suppressed by overexpression of TRPML1. Notably, this PI(3,5)P_2-dependent regulation of TRPML1 is evolutionarily conserved. In budding yeast, hyperosmotic stress induces Ca^{2+} release from the vacuole. Here, we show that this release requires both PI(3,5)P_2 production and a yeast functional TRPML homolog. We propose that TRPMLs regulate membrane trafficking by transducing information about PI(3,5)P_2 levels into changes in juxtaorganellar Ca^{2+}, thereby triggering membrane fusion/fission events.

Keywords

Whole-endolysosome recording; TRP channel; Ca^{2+} release channel; PIKfyve; Fab1; phosphoinositide; PI(3,5)P_2; type IV Mucolipidosis; endosome; lysosome; membrane trafficking; vacuole

[*]To whom correspondence should be addressed: haoxingx@umich.edu.
[#]These authors contributed equally to this work.

Author Contributions

X.P.D., D.S., and X.W. contributed equally to this work. H.X., M.D., and X.P.D. designed research; X.P.D., D.S., X.W., T.D., and Z.Q. performed research. X.L., X.C., Y.Z., L.S.W., M.D. contributed new regents; X.P.D., D.S., X.W., T.D., Z.Q., and H.X. analyzed the data; and H.X., X.P.D., and D.S. wrote the paper.

Competing financial interests

The authors declare no competing financial interests.

Introduction

Ca^{2+} is a key regulator of synaptic vesicle fusion during neurotransmission. Similarly, Ca^{2+} is thought to regulate other, more general membrane trafficking pathways [1]. However, in these cases, the source of Ca^{2+} is unknown. For these general pathways, it has been postulated that Ca^{2+} is released through unidentified Ca^{2+} channels from the lumen of vesicles and organelles [1–3]. Transient receptor potential (TRP) proteins are a superfamily of Ca^{2+}-permeable cation channels that are localized at the plasma membrane and/or membranes of intracellular organelles [4]. For example, mucolipin TRPs (TRPML1-3) are localized in the membranes of endosomes and lysosomes (collectively endolysosomes) [5–6]. Mutations in the human *TRPML1* gene cause mucolipidosis type IV (ML4) neurodegenerative disease [7–8]. Cells that lack TRPML1 exhibit enlarged endolysosomes and trafficking defects in the late endocytic pathway (reviewed in Refs. [5–6]). TRPMLs are, therefore, natural candidate channels for Ca^{2+} release in the endolysosome.

$PI(3,5)P_2$ is a low-abundance endolysosome-specific phosphoinositide [9–12]. $PI(3,5)P_2$ can be generated from PI(3)P through PIKfyve/Fab1, a PI 5-kinase that is localized in the endolysosome of both yeast and mammalian cells [11,13–15]. The activity of PIKfyve/Fab1 can be positively regulated by several associated proteins such as Fig4, Vac14, and Vac7 [10–12, 16]. On the other hand, $PI(3,5)P_2$ can be metabolized into PI(5)P through the myotubularin (MTM/MTMR)-family of PI-3 phosphatase [11,15,17]. Human mutations in $PI(3,5)P_2$-metabolizing enzymes and their regulators cause a variety of neurodegenerative diseases including amyotrophic lateral sclerosis (ALS) and Charcot-Marie-Tooth (CMT) disease [10–11,18]. At the cellular level, $PI(3,5)P_2$-deficient cells reportedly exhibit enlarged endolysosomes/vacuoles and trafficking defects in the endocytic pathways [10–12,16].

Because the cellular phenotypes in $PI(3,5)P_2$-deficient cells are similar to those observed in cells lacking TRPML1, we hypothesized that TRPML1 may act as an endolysosomal Ca^{2+}-release channel that is regulated by $PI(3,5)P_2$. In this study, by direct patch-clamping of the endolysosomal membrane, we have found that $PI(3,5)P_2$ activates TRPMLs with striking specificity and potency. Protein-lipid interaction and mutational analyses revealed that $PI(3,5)P_2$ binds directly to the N-terminus of TRPML1. Overexpression of TRPML1 suppresses the enlarged vacuole phenotype observed in $PI(3,5)P_2$-deficient cells. We conclude that $PI(3,5)P_2$ controls endolysosomal membrane trafficking by regulating TRPML channels to change juxtaorganellar Ca^{2+} levels.

Results

Activation of endolysosomal TRPML channels by $PI(3,5)P_2$

TRPML1 is primarily localized on membranes of late endosomes and lysosomes (LELs) [5, 19] (see Supplementary Fig. S1), which are inaccessible to conventional electrophysiological approaches. Using our recently-established modified patch-clamp method [4,20], we performed recordings directly on native LEL membranes. HEK293T or Cos-1 cells were transfected with either EGFP-TRPML1 alone, or co-transfected with mCherry-TRPML1 and EGFP-Lamp1 (a marker for LEL). Whole-endolysosome recordings (see Fig. 1a; note that the inward current indicates cations flowing out of the endolysosome) were performed on enlarged vacuoles manually isolated from cells pre-treated with vacuolin-1 [21], which caused an increase in the diameter of the vacuoles from < 0.5 μm to up to 5 μm (mean capacitance = 0.68 ± 0.05 pF, N = 44 vacuoles). The majority (>85%) of mCherry-TRPML1-positive vacuoles were also EGFP-Lamp1-positive, confirming that the TRPML1-positive vacuoles were enlarged LELs [21]. In the TRPML1-positive enlarged LELs, small basal inwardly rectifying currents (72 ± 12 pA/pF at −140 mV, N = 65 vacuoles) were seen under the whole-endolysosome configuration (Fig. 1b, 1c). Bath application of 100 nM $PI(3,5)P_2$ in a water-soluble diC8 form, rapidly and

dramatically activated TRPML1-mediated current (I_{TRPML1}; τ= 15 ± 4 s at −140 mV, N = 8 vacuoles; 18.3 ± 2.7-fold increase of basal activity, N = 20 vacuoles) (Fig. 1b–f). PI(3,5)P_2-dependent activation was dose-dependent (EC_{50}= 48 ± 14 nM, Hill slope (n) = 1.9, N = 7 vacuoles). On average, I_{TRPML1} in the presence of 100 nM diC8 PI(3,5)P_2 was 982 ± 150 pA/pF at −140 mV (N = 23 vacuoles). Full-length diC16 PI(3,5)P_2 appeared to be less effective, presumably because of its low aqueous solubility (Supplementary Fig. S2). Therefore, diC8 PI(3,5)P_2 was used for electrophysiological studies hereafter.

In yeast, PI(3,5)P_2 is exclusively produced from PI(3)P by the PIKfyve/Fab1 PI 5-kinase (see Supplementary Fig. S1) [9,22–23]. PI(3,5)P_2 can be quickly metabolized into PI(3)P by Fig4, or to PI(5)P by MTMR-family phosphatases [11,13,17,24]. Neither PI(3)P (1 μM; 1.05 ± 0.17 fold increase of basal, N = 4; Fig. 1e, 1f) nor PI(5)P (1 μM; 0.98 ± 0.05 fold increase of basal, N=3; Fig. 1f) activated I_{TRPML1}. PI(3)P and PI(3,5)P_2 are localized in the endolysosome system. Other PIPs such as PI(3,4)P_2, PI(4,5)P_2, and PI(3,4,5)P_3, are localized in the plasma membrane, or in other intracellular organelles, and are sequestered from endolysosomes [15]. I_{TRPML1} was not activated by these other PIPs (Fig. 1f & Supplementary Fig. S3). Thus, PI(3,5)P_2 activated I_{TRPML1} with a striking specificity. TRPML2 and TRPML3 are also localized in the endolysosome [5]. PI(3,5)P_2, but not PI(3)P (data not shown) activated whole-endolysosome I_{TRPML2} (Fig. 1g) and I_{TRPML3} (Fig. 1h). Since PI(3,5)P_2 and TRPMLs are both primarily localized in the LEL (Refs. [5, 11]; see Supplementary Fig. S4), the insensitivity of I_{TRPML1} to PI(3)P or PI(5)P, and its robust activation by PI(3,5)P_2 suggested that TRPML1 might be acutely regulated by the activities of PIKfyve/Fab1, or by Fig4 or MTMR phosphatases in the LEL.

PI(3,5)P_2-mediated activation gating of TRPML1

To explore the mechanisms underlying PI(3,5)P_2-dependent activation of TRPMLs, we tested the effect of PI(3,5)P_2 on several gain-of-function mutations in TRPML1 channels [20]. Recently, we and others found that a spontaneous mutation (*Varitint Waddler*; *Va*) in the 5th transmembrane domain of TRPML3 dramatically increased TRPML3 channel activity (Refs. [5–6]). Further analysis suggested that *Va* is a gating mutation that locks TRPML1-3 channels in an open non-gating state [5–6]. In contrast with I_{TRPML1}, whole-endolysosome $I_{TRPML1\text{-}Va}$ exhibited large basal currents (1,190 ± 254 pA/pF at −140 mV, N = 5), that failed to increase with PI(3,5)P_2 application (0.99 ± 0.01 of basal, N = 3; Fig. 1i, 1k, 1l). TRPML1-R427P is a partial gain-of-function mutation [20]. Whole-endolysosome $I_{TRPML1\text{-}R427P}$ exhibited a substantial basal current (349 ± 80 pA/pF at −140 mV, N = 3), but was only modestly activated by PI(3,5)P_2, at 3.7 ± 1.3 fold of basal activity (N = 7) (Fig. 1j–l). Collectively, these results suggested that PI(3,5)P_2 activated TRPML1 by increasing the open probability.

Activation of endogenous TRPML-like currents by PI(3,5)P_2

Next, we investigated whether PI(3,5)P_2 activated endogenous TRPMLs. Using enlarged LELs isolated from non-transfected Cos-1 cells, we were able to record PI(3,5)P_2–activated, inwardly rectifying TRPML-like currents ($I_{TRPML\text{-}L}$) in 4 out of 20 vacuoles (Fig. 2a). $I_{TRPML\text{-}L}$ was 68 ± 4 pA/pF at −140 mV (N = 4). In enlarged LELs isolated from wild-type (TRPML1$^{+/+}$) human fibroblast cells, however, PI(3,5)P_2–activated $I_{TRPML\text{-}L}$ was detected in 5 of 5 tested vacuoles (Fig. 2b), with an average current amplitude larger than Cos-1 cells (239 ± 37 pA/pF at −140 mV, N = 5; Fig. 2d). In contrast, enlarged LELs from human ML4 (TRPML1$^{-/-}$ or abbreviated as ML1$^{-/-}$) fibroblasts showed no significant PI(3,5)P_2–activated $I_{TRPML\text{-}L}$ (15.7 ± 5.2 pA/pF at −140 mV, N = 6; Fig. 2c, 2d). These results indicated that PI(3,5)P_2 activated endogenous TRPMLs, and that TRPML1 was the primary or sole functional TRPML channel in the endolysosome of human fibroblast, although a previous study reported the expression of TRPML2 and TRPML3 in human fibroblasts [25].

Suppression of I_{TRPML1} by a decrease in $PI(3,5)P_2$

Whole-endolysosome I_{TRPML1} exhibited a decay or slow return to steady-state levels upon washout of diC8 $PI(3,5)P_2$ (Fig. 3a). If $PI(3,5)P_2$ levels underlie the basal pre-$PI(3,5)P_2$, or the post-$PI(3,5)P_2$ activity of TRPML1, diminishing the $PI(3,5)P_2$ level would be expected to decrease the I_{TRPML1}. One method of "chelating" PIPs is adding polycations such as poly-lysine to the cytoplasmic side of the membrane, where they bind the negatively-charged phosphate head groups of PIPs in an electrostatic manner [26–27]. Poly-lysine at 500 μg /ml rapidly inhibited post-$PI(3,5)P_2$ I_{TRPML1}, but not $I_{TRPML1\text{-}Va}$ (Fig. 3a–c), indicating that poly-lysine primarily affected TRPML1 (activation) gating. In support, a neutralizing anti- $PI(3,5)P_2$ antibody at 5 μg /ml significantly inhibited post-$PI(3,5)P_2$ I_{TRPML1}, but not $I_{TRPML1\text{-}Va}$ (Fig. 3d–f). In contrast, no significant inhibition was seen with an anti-$PI(4,5)P_2$ antibody (Fig. 3d, 3e). To further investigate whether the basal I_{TRPML1} prior to $PI(3,5)P_2$ treatment was caused by basal levels of $PI(3,5)P_2$ in the endolysosomal membrane, we investigated a subset of vacuoles with large basal currents of > 100 pA at −140 mV. Strong inhibitions were seen with poly-lysine (92 ± 1%, N = 7) or anti-$PI(3,5)P_2$ antibody (94 ± 1%, N = 10), but not with anti-$PI(4,5)P_2$ antibody (3 ± 1%, N = 4; Fig. 3g–i).

To further confirm that $PI(3,5)P_2$ is an endogenous activator of TRPML1, we also recorded basal I_{TRPML1} after depleting the $PI(3,5)P_2$ level by overexpressing MTM1, a PI-3 phosphatase that can convert $PI(3,5)P_2$ and PI(3)P into PI(5)P and PI, respectively [11,15]. A rapamycin-dependent heterodimerization system was used to recruit the otherwise cytosolic MTM1 28 (see Fig. 4a, 4b). In cells expressing both RFP-FRB-MTM1 and EGFP-2*FKBP-Rab7, rapamycin induced a rapid recruitment of MTM1 to Rab7-positive LEL membranes (Fig. 4b). We noticed that the basal $I_{TRPML1}$was consistently larger for vacuoles isolated from Cos-1 cells with longer (> 5h) pretreatment of vacuolin-1 (data not shown). In vacuoles isolated from MTM1-transfected cell, large basal I_{TRPML1} was seen before rapamycin treatment (Fig. 4c). Following recruitment of MTM1 (Fig. 4d), but not the inactive mutant (C375S) MTM1 (Fig. 4e), however, a large suppression of basal whole-endolysosome I_{TRPML1} was seen (Fig. 4d–f). Collectively, these results suggested that $PI(3,5)P_2$ levels were the primary determinant of TRPML1 channel activity in the endolysosome.

Binding of $PI(3,5)P_2$ to the N-terminus of TRPML1 *in vitro*

Phosphoinoitides are known to bind with high affinity to PI-binding modules such as PH or FYVE domain, or to poly-basic region with unstructured clusters of positively-charged amino acid residues, such as Arg and Lys, in an electrostatic manner [27]. $PI(4,5)P_2$ can bind directly to the cytoplasmic N- and C- termini of several plasma membrane TRPs [26,29]. Notably, the intracellular N terminus of TRPML1 has a poly-basic region [26] (see Fig. 5a). To test whether $PI(3,5)P_2$ binds directly to TRPML1, we fused GST to the entire N-terminus of mouse TRPML1, up to residue 69 (see Fig. 5a for putative membrane topology). The protein, GST-TRPML1-N (abbreviated as GST-ML1-N), was used to probe phosphoinositides immobilized on a nitrocellulose membranes [26–27,29]. GST-ML1-N, but not GST alone, bound to PIP_3 and PIP_2s, but not to other PIPs or phospholipids (Fig. 5b). A liposome assay showed that GST-ML1-N strongly associated with $PI(3,5)P_2$, but not PI(3)P or control liposomes (Fig. 5c). In a pull-down assay, agarose beads conjugated with $PI(3,5)P_2$, but not control lipids, pulled down GST-ML1-N (Fig. 5d). Taken together, these results suggested that $PI(3,5)P_2$ bound directly *in vitro* to the cytoplasmic N-terminus of TRPML1.

Critical amino-acid residues in $PI(3,5)P_2$ binding

To further map the $PI(3,5)P_2$ binding sites, we systematically replaced positively-charged amino acid residues (Arg and Lys) within and adjacent to the poly-basic region with non-charged Gln residues and assayed Gln-substituted, purified GST-fusion proteins for PI(3,5)P_2 binding. We also tested whether $PI(3,5)P_2$ activated Gln-substituted TRPML1 channels

using whole-endolysosome recordings. A most dramatic decrease in $PI(3,5)P_2$ binding and activation (Fig. 5e–g) was observed in a 7Q mutant, with seven substitutions (R42Q/R43Q/R44Q/K55Q/R57Q/R61Q/K62Q; Fig. 5a). In contrast to GST-ML1-N, GST-ML1-7Q-N failed to bind significantly to $PI(3,5)P_2$ or to other PIPs in the PIP strip and pull down assays (Fig. 5b, 5e). Considering the specificity of $PI(3,5)P_2$ for TRPML1 activation, one plausible explanation for the apparent discrepancy between our biochemical assays (see Fig. 5b) and electrophysiological measurements (see Fig. 1f) is that the purified GST-ML1-N protein fragment did not recapitulate the specificity of PIP-binding of full length TRPML1 in the endolysosomal membrane. Nevertheless, the binding affinity of ML1-N to $PI(3,5)P_2$ was dramatically reduced by removing the charges with the 7Q mutations (Fig. 5e), suggesting that multiple positively charged amino acid residues are critical for $PI(3,5)P_2$ binding.

Compared to wild type (WT) TRPML1, TRPML1-7Q was only weakly activated by high concentrations of $PI(3,5)P_2$, with a maximal response (efficacy) that was approximately 20% of I_{TRPML1} (EC_{50}= 2.2 ± 2 μM, Hill slope (n) = 0.8, N = 6 vacuoles) (Fig. 5f, 5g). Like $TRPML1^{Va}$, $TRPML1^{Va}$–7Q also exhibited large basal currents (Fig. 5h), suggesting a relatively specific effect of 7Q mutations on $PI(3,5)P_2$-dependent activation. Consistent with the $PI(3,5)P_2$ binding-assay results, we found that GST-ML1-N, but not GST-ML1-7Q-N, competitively reduced the activation effect of $PI(3,5)P_2$ (Fig. 5i, 5j). Collectively, our results suggested that $PI(3,5)P_2$ bound directly to the cytoplasmic N-terminus of TRPML1, resulting in conformational changes that favor opening of TRPML1.

$PI(3,5)P_2$ in vacuolar Ca^{2+} release in yeast

TRPML1 is a Ca^{2+}-permeable channel [30–31], so activation by $PI(3,5)P_2$ may lead to Ca^{2+} release from endolysosomes. Although PIKfyve/Fab1 is a PI 5-kinase responsible for $PI(3,5)P_2$ generation in both yeast and mammalian cells [11,13–15], the extracellular signals that lead to activation of PIKfyve in mammalian cells have not been identified. Furthermore, endolysosomal Ca^{2+} release has been difficult to detect in mammalian cells because of the small size of the endolysosome [5,32]. In contrast, Fab1-mediated $PI(3,5)P_2$ production has been well documented in yeast [11,13]. For example, hyperosmotic shock increases $PI(3,5)P_2$ levels more than 20-fold within a few minutes [11,13]. Interestingly, hyperosmotic shock is also known to induce Ca^{2+} release from yeast vacuoles, which share many similar features with mammalian lysosomes. Induction of Ca^{2+} release is through Yvc1/TRPY1, a TRP-channel homolog in yeast, and occurs with a slightly faster, but otherwise comparable time-course of $PI(3,5)P_2$ elevation [33]. Based on our data, we hypothesized that hyperosmolarity-induced vacuolar Ca^{2+} release would be dependent on elevated $PI(3,5)P_2$ levels. To test this, we used an a luminescence assay based on aequorin, a genetic Ca^{2+} sensor, [33] to measure changes in cytosolic Ca^{2+} ($[Ca^{2+}]_{cyt}$) levels. Consistent with previous reports [33], hyperosmotic shock by addition of 0.9 M NaCl to the culture medium induced a rapid and dramatic increase of $[Ca^{2+}]_{cyt}$. The time required for peak $[Ca^{2+}]_{cyt}$ increase was 48 ± 4 sec, (N = 10 yeast colonies/experiments); the increase of luminescence was 700 ± 94% over basal (N = 4; Fig. 6a, 6b). In the *yvc1*Δ mutant, however, no significant increase in $[Ca^{2+}]_{cyt}$ was seen (29 ± 6 % over basal, N = 4), consistent with the hypothesis that the $[Ca^{2+}]_{cyt}$ increase resulted primarily from vacuolar release through Yvc1[33]. Interestingly, in the *fab1*Δ mutant, hyperosmotic shock also failed to induce any significant increase in $[Ca^{2+}]_{cyt}$ (20 ± 8 %, N = 4; Fig. 6a, 6b), in comparison with 700 % for the wild-type cells. Both *yvc1*Δ and *fab1*Δ cells responded to 14% ethanol or 0.03 % SDS (data not shown), which is known to induce Ca^{2+} influx [33]. Consistent with previous studies [11,13], *fab1*Δ mutant yeasts failed to exhibit vacuolar fragmentation in response to hyperosmotic shock (Fig. 6c).

Fab1 kinase activity is regulated by Vac7, Vac14 and Fig4, mutations in which cause a partial or nearly complete loss of Fab1-mediated $PI(3,5)P_2$ production [11–13,15,34]. All these mutants

exhibited reduced vacuolar Ca^{2+} release: 533 ± 60 % (N = 4) for *fig4*Δ, 357 ± 77 % (N = 4) for *vac14*Δ, and 106 ± 18 % (N = 4) for *vac7*Δ (Fig. 6a, 6b). The degree of Ca^{2+}-release reduction (*fab1*Δ > *vac7*Δ>*vac14*Δ> *fig4*Δ) correlated well with the severity of the defect of $PI(3,5)P_2$ production in these strains [11]. The loss of Ca^{2+} response in *fab1*Δ cells was not due to reduced expression of Yvc1 (Fig. 6d, 6e), as transformation of Yvc1-GFP failed to restore the response. In contrast, when wild-type yeast *FAB1* was transformed into *fab1*Δ mutant yeast, hyperosmolarity-induced $[Ca^{2+}]_{cyt}$ increase was largely restored (Fig. 6f, 6g). Mutant *fab1*Δ yeast reportedly hypo-acidify the vacuole [11,13], which could result in reduced Ca^{2+} release because of a decrease in H^+-dependent refilling of vacuolar Ca^{2+} stores mediated by Vcx1 (vacuolar Ca^{2+}-H^+ exchanger) [35]. However, *vcx1*Δ cells exhibit normal Ca^{2+} release in response to hyperosmotic shock [33], indicating that the alternate Pmc1 (vacuolar Ca^{2+} ATPase)-mediated refilling system is sufficient to maintain vacuolar Ca^{2+} stores. In support, we found that hypo-acidified cells lacking *vma3*, an essential component of the vacuolar ATPase [35], exhibited normal $[Ca^{2+}]_{cyt}$ release (Fig. 6h). These results suggested that the Fab1-mediated $PI(3,5)P_2$ generation system was required for hyperosmolarity-induced, Yvc1-dependent vacuolar Ca^{2+} release. Although TRPML1 shares a degree of sequence homology to Yvc1, they differ significantly in their channel properties [5,36]. To test whether TRPML1 functions in yeast, we overexpressed TRPML1 in both a wild-type and *yvc1*Δ background. Overexpression of TRPML1 in wild-type yeast resulted in a significant increase in Ca^{2+} release in response to hyperosmotic shock (Fig. 6i, 6j). In *yvc1*Δcells, overexpression of TRPML1, but not a non-functional pore mutant of TRPML1 (TRPML1-KK), resulted in a partial rescue of the $[Ca^{2+}]_{cyt}$ response, with a 114 ± 14% increase over basal luminescence (N = 9) (Fig. 6k). In contrast, overexpression of TRPML1 in *fab1*Δ failed to result in significant $[Ca^{2+}]_{cyt}$ response (Supplementary Fig. S5), while overexpression of YVC1 in *yvc1*Δcells completely restored the $[Ca^{2+}]_{cyt}$ response (Supplementary Fig. S6). The rescue might be incomplete because Yvc1, but not TRPML1, is activated by cytoplasmic Ca^{2+} and mechanical force [36], both of which might have synergistic effects with $PI(3,5)P_2$. Nevertheless, these results suggested that regulation of lysosomal Ca^{2+} channels by $PI(3,5)P_2$ might be a conserved mechanism in eukaryotic cells.

TRPML1 and $PI(3,5)P_2$ in endolysosomal trafficking

The data presented here suggest that TRPMLs might be activated downstream of the $PI(3,5)P_2$ increase, to trigger membrane fusion and fission (see Supplementary Fig. S1). If this hypothesis is correct, expression of TRPML1, which often exhibits substantial basal activity in heterologous systems [5], might alleviate trafficking defects in $PI(3,5)P_2$-deficient cells. In cultured $Vac14^{-/-}$ fibroblast cells, the trafficking defects from $PI(3,5)P_2$ deficiency were reflected by enlarged vacuoles/LELs (> 3 up to 12 μm in diameter) in 79 ± 7% of the cells (N = 3 experiments with >100 cells) (Fig. 7a; Ref. 12). Only approximately 5–10 % of WT cells were vacuolated (< 4 μm; data not shown). Transfection of a wild-type Vac14 construct was sufficient to restrict vacuoles to 15 ± 2% of cells (N = 3 experiments; Fig. 7a). Interestingly, we were able to rescue the vacuolar phenotype by transfection of TRPML1, which showed vacuolation in 18 ± 1 % cells (N = 6), but not pore-mutant TRPML1 (ML1-KK) with 69 ± 6% vacuolation (N = 3), or the $PI(3,5)P_2$-insensitive mutant TRPML1 (ML1-7Q) with 75 ± 7% vacuolation (N = 3) (Fig. 7a–d). Although ML1-7Q still localized to Lamp1-positive compartments (Fig. 7b, 7e), large vacuoles were seen in the majority of ML1-7Q-transfected $Vac14^{-/-}$ fibroblasts (Fig. 7a–d). Collectively, these results suggested that TRPML1 channel activity and $PI(3,5)P_2$ sensitivity played important roles in controlling vacuole size.

Discussion

We used biochemical binding assays to demonstrate that $PI(3,5)P_2$ binds directly to the N-terminus of TRPML1. Using whole-endolysosomal patch-clamp recordings, we showed that

$PI(3,5)P_2$ robustly activates TRPML1 in the endolysosome. The effect of $PI(3,5)P_2$ was strikingly specific; none of the other PIPs activated TRPML1. Using a spectrum of yeast mutant strains with variable degrees of $PI(3,5)P_2$ deficiency, we established a high-degree of correlation between the amount of vacuolar Ca^{2+} release and the levels of $PI(3,5)P_2$. Finally, we showed that overexpression of WT, but not the PIP_2-insensitive variant of TRPML1, was sufficient to rescue the trafficking defects in $PI(3,5)P_2$-deficient mammalian cells, as demonstrated by observation of enlarged vacuoles. Our identification of an endolysosome-localizing Ca^{2+} channel that is activated by the endolysosome-specific $PI(3,5)P_2$ provides a previously unknown link between these two important regulators of intracellular membrane trafficking.

Similar trafficking defects are seen in both $TRPML1^{-/-}$, and $PI(3,5)P_2$-deficient cells. For example, LEL-to-Golgi retrograde trafficking, a process requiring membrane fission, is defective in both $TRPML1^{-/-}$ cells [5,19,37–39], and in $PI(3,5)P_2$-deficient cells [11–15,34]. Furthermore, both TRPML1 and $PI(3,5)P_2$-metabolizing enzymes are implicated in membrane-fusion processes like exocytosis [11,15,20], and lysosomal fusion with autophagosomes [6,40]. Thus, both TRPML1 and $PI(3,5)P_2$ play active roles in membrane fission and fusion. However, the cellular defects of $PI(3,5)P_2$-deficient cells are generally more severe than $TRPML1^{-/-}$ cells. $PI(3,5)P_2$ is proposed to have at least five independent functions, including: recruitment of cytosolic proteins to define organelle specificity; functional regulation of endolysosomal membrane proteins; determination of physical properties and fusogenic potential of endolysosomal membranes; serving as precursor for PI(3)P or PI(5)P, and modulation of endolysosomal pH [9,11,15]. Hence, activation of TRPML1 might define a subset of the multiple functions of $PI(3,5)P_2$. Such activation, however, may provide an essential spatial and temporal regulation of endolysosomal dynamics. Membrane fusion and fission are highly coordinated processes requiring an array of cytosolic and membrane-bound proteins and factors. A local increase in $PI(3,5)P_2$ likely recruits protein complexes required to generate the membrane curvature necessary for membrane fusion and fission [15]. A local increase in $PI(3,5)P_2$ could also activate TRPML1 to elevate juxtaorganellar Ca^{2+}, which binds to a putative Ca^{2+} sensor protein such as Synaptotagmin/CaM [3] or ALG-2 [41], to exert effects on SNARE proteins or lipid bilayer fusion [15,42]. A similar mechanism might be employed by NAADP and TPC channels to regulate membrane trafficking in the endolysosome[32,43].

The remarkable specificity of $PI(3,5)P_2$ in activating TRPML1 is consistent with the role of Ca^{2+} in controlling the direction and specificity of membrane traffic [1,3]. Although we identified several positively charged amino acid residues as potential $PI(3,5)P_2$ binding sites, electrostatic interaction alone is unlikely to provide a high affinity $PI(3,5)P_2$ binding pocket [26–27]. Thus, additional structural determinants such as hydrophobic amino acid residues must also contribute to specificity, by interacting with the lipid portion of $PI(3,5)P_2$. Because of the low abundance of $PI(3,5)P_2$ [11], such specificity might be a pre-requisite for $PI(3,5)P_2$ and TRPML1 to control the trafficking direction in the late-endocytic pathway. In other organelles, however, other PIPs and intracellular Ca^{2+} channels are likely to provide machinery necessary for Ca^{2+}-dependent membrane fission and fusion. Within LELs, membrane fusion and fission are likely to occur in sub-organellar compartments that are enriched for both TRPMLs and PIKfyve. While TRPML-mediated juxtaorganellar Ca^{2+} transients might be captured using real-time live-imaging methods, these seemingly “spontaneous” events may correlate with membrane fusion and fission events that can be simultaneously monitored with fluorescence-imaging approaches.

Methods

Molecular biology and biochemistry

Full-length mouse TRPML1, 2, and 3 were cloned into the EGFP-C2 (Clontech) or mCherry vector 20¯21,31. TRPML1 non-conducting pore mutant (D471K/D472K; abbreviated TRPML1-KK) and PIP_2-insensitive mutant (R42Q/R43Q/R44Q/K55Q/R57Q/R61Q/K62Q; abbreviated TRPML1-7Q) were constructed using a site-directed mutagenesis kit (Qiagen). For glutathione S-transferase (GST) fusion constructs, DNA fragments corresponding to the N- (amino acid residues 1–69) terminal regions of mouse TRPML1 were generated by PCR amplification and cloned into the Eco*RI* and Xho*I* site of pGEX4T1, in frame to generate GST-fusion protein plasmids (pGEX-ML1-N). For overexpression of TRPML1 in yeast, full-length mouse TRPML1 was cloned into the Xho*I* and Eco*RI* site of the pCuGFP416 vector, and the XhoI and Hind III site of the pVT102U-GFP vector. FKBP*2 fragment was PCR-amplified from EGFP-FKBP12-Rab5 and inserted into the HindIII and XhoI site of EGFP-Rab7 vector. RFP-FRB-MTM1 and EGFP-FKBP*2-Rab5 were kind gift from Dr.Banasfe Larijani. All constructs were confirmed by sequencing, and protein expression was verified by Western blot. HEK293T, Cos-1, human fibroblasts, or mouse primary fibroblast cells were transiently transfected with TRPML1-3 and the TRPML1 mutants for electrophysiology, biochemistry, live-cell imaging, and confocal imaging. Confocal images were taken using a Leica (TCS SP5) microscope. TRPML1 Western blot analyses were performed with an anti-GFP monoclonal antibody (Covance).

Endolysosomal electrophysiology

Endolysosomal electrophysiology was performed in isolated endolysosomes using a modified patch-clamp method 20–21. HEK293 or Cos-1 cells were used for all the heterologous expression experiments and were transfected using Lipofectamine 2000 (Invitrogen) with TRPML1 or mutants fused to GFP or mCherry. Human skin fibroblast cells from a ML4 patient ($TRPML1^{-/-}$, clone GM02048) and age-matched control ($TRPML1^{+/+}$, clone GM00969) were obtained from the Coriell Institute for Medical Research (NJ, U.S.A). LEL size is usually < 0.5 μm, which is suboptimal for patch clamping. We therefore treated cells with 1 μM vacuolin-1, a lipid-soluble polycyclic triazine that can selectively increase the size of endosomes and lysosomes, for ~1h [44]. Large vacuoles (up to 5 μm; capacitance = 0.68 ± 0.05 pF, N = 44 vacuoles) were observed in most vacuolin-treated cells. Occasionally, enlarged LELs were obtained from TRPML1-transfected cells without vacuolin-1 treatment. No significant difference in TRPML channel properties were seen for enlarged LELs obtained with or without vacuolin-1 treatment. Vacuoles positive for both mCherry-TRPML1 and EGFP-Lamp1 were considered enlarged LELs. Whole-endolysosome recordings were performed on isolated enlarged LELs. In brief, a patch pipette (electrode) was pressed against a cell and quickly pulled away to slice the cell membrane. Enlarged LELs were released into a dish and identified by monitoring EGFP-TRPML1, the mCherry-TRPML1 or EGFP-Lamp1 fluorescence. Unless otherwise stated, bath (internal/cytoplasmic) solution contained 140 mM K-Gluconate, 4 mM NaCl, 1 mM EGTA, 2 mM Na_2-ATP, 2 mM $MgCl_2$, 0.39 mM $CaCl_2$, 0.1 mM GTP, 10 mM HEPES (pH adjusted with KOH to 7.2; free $[Ca^{2+}]_i$ approximately 100 nM). Pipette (luminal) solution was pH 4.6 standard extracellular solution (modified Tyrode's) with 145 mM NaCl, 5 mM KCl, 2 mM $CaCl_2$, 1 mM $MgCl_2$, 20 mM HEPES, 10 mM glucose (pH adjusted with NaOH). All bath solutions were applied via a fast perfusion system to achieve a complete solution exchange within a few seconds. Data were collected using an Axopatch 2A patch clamp amplifier, Digidata 1440, and pClamp 10.0 software (Axon Instruments). Whole-endolysosome currents were digitized at 10 kHz and filtered at 2 kHz. All experiments were conducted at room temperature (21–23°C), and all recordings were analyzed with pCLAMP10 (Axon Instruments, Union City, CA), and Origin 8.0 (OriginLab, Northampton, MA). All PIP antibodies are from Echelon Biosciences Inc. All PIPs are from A.G. Scientific, Inc.

GST fusion proteins

To purify GST-tagged proteins, *Escherchia coli* BL21DE3 was transformed with empty pGEX vectors or pGEX-TRPML1-N (abbreviated as pGEX-ML1-N). After growth to approximately OD_{600} = 0.6 in a SuperBroth medium supplemented with ampicillin, expression was induced with IPTG (1 mM) for 7 h at 37°C. Cells were collected and resuspended in 30 ml of ice-cold PBS supplemented with protease inhibitor cocktail, 0.5 mM EDTA, and deoxytibonuclease, and lysed with a French press. Cell lysates in 1% Triton-X100 were incubated with 2 mL mixed glutathione Sepharose (GE Healthcare) for 1 h at 4°C. After three washes with 30 mL PBS, proteins were eluted with 7 mL elution buffer (10 mM Glutathione, 50 mM Tris, pH 8).

Lipid Strip Binding Assay

Lipid binding analysis of GST-ML1-N and GST-ML1-7Q-N fusion proteins was conducted using PIP Strips (Echelon Biosciences Inc.), with each spot containing 100 pmol active lipids. Membranes were blocked with Phosphate Buffered Saline Tween (PBST) solution (supplemented with 3% fatty acid-free bovine serum albumin) for 1 h at room temperature, and incubated with 0.5–3 μg GST-fusion protein in blocking buffer overnight. After six washes, the membranes were incubated with a mouse anti-GST antibody (1:5000, Sigma) for 1 h at room temperature, and secondary antibody HRP-labeled goat anti-mouse (1:5000) was added before detection by enhanced chemiluminescence.

PIP bead binding assay

Purified GST fusion proteins (10 μg) were diluted in 1 mL binding buffer (50 mM Tris, 150 mM NaCl, 0.25% NP-40, pH 7.5) and incubated with 50 μl of 50% lipid-conjugated Sepharose beads (Echelon Biosciences Inc.) for 2 h. After three washes, proteins were eluted from the PIP beads by heating at 50°C for 10 min in 2X SDS-PAGE sample buffer and visualization by Western blot.

Liposome binding assay

Purified GST fusion proteins (3 μg) were incubated with 20 μl liposome (Echelon Biosciences Inc.) in 1 mL binding buffer (50 mM Tris, 150 mM NaCl, 0.05% Nonidet P-40, pH 7.5) for 10 min. Liposomes were pelleted at 16,000 × *g* for 10 min and washed multiple times with binding buffer. Bound fractions were analyzed by Western blot.

Yeast Strains

Wild-type and mutant yeast strains are listed in Table 1. Strains were grown at 24°C or 30°C in either YPD (yeast extract/peptone/glucose) or synthetic complete (SC) minimal medium.

Yeast Ca^{2+} imaging

Yeast Ca^{2+} imaging experiments were performed using an aequorin-based genetic Ca^{2+} sensor method [33]. PEVP11/AEQ plasmid was kindly provided by Dr. Patrick H. Masson (University of Wisconsin-Madison, Madison, WI). Transformed yeasts were inoculated from a saturated overnight culture to OD_{600} ~ 0.3 in a synthetic defined (SD) medium with 3 μM coelenterazine, and grown overnight (OD_{600} = 2–3) at 24°C or 30°C to convert apo-aequorin to aequorin. For each experiment, an aliquot of 250 μl was harvested, re-suspended in 100 μl SD medium, and transferred to 94-well plates for luminescence measurement. Baseline luminescence was recorded every 3 s for 30 s using a PHERAstar plate reader (BMG Labs). Hyperosmotic shock was performed by adding an equal volume of SD medium (100 μl) containing 1.8 M NaCl to a final concentration of 0.9 M. All experiments were concluded with 14% ethanol or 0.03 % SDS, which resulted in maximal luminescence and served as a positive control for aequorin transformation.

Yeast vacuole labeling

Log-phase yeast cells were labeled with FM4-64 dye (Molecular Probes) [34]. Phase contrast and fluorescence images were taken using a Zeiss microscope with a 100X objective.

Mouse fibroblast vacuole assay

Vac14$^{-/-}$ mouse fibroblast cells were isolated and cultured as described previously [12]. Briefly, fibroblasts were transiently transfected by electroporation (260 V, 950 μF) with 100 μg of the following expression constructs: mCit, mCit-Vac14, GFP-ML1, GFP-ML1-KK, or GFP-ML1-7Q. Cells were grown on 100-mm plates to 90% confluence and distributed to six 35-mm plates after electroporation. Cells were fixed with 4% paraformaldehyde 24 h after electroporation. Fibroblasts were considered to be vacuolated if they had at least one enlarged (> 3 μm) cytoplasmic vacuole.

Cellular fractionation

To perform lysosomal fractionation studies [45], cell lysates were obtained by Dounce homogenization in a homogenizing buffer (0.25 M sucrose, 1 mM Na_2EDTA, 10 mM HEPES, pH 7.0). Lysates were then centrifuged at 1900 × *g* at 4°C for 10 min to remove the nuclei and intact cells. Post-nuclear supernatants underwent ultracentrifugation through a Percoll density gradient using a Beckman L8-70 ultracentrifuge. An ultracentrifuge tube was layered with 2.5 M sucrose, 18% Percoll in homogenizing buffer, and the post-nuclear supernatant on top. Centrifugation was 67,200 × *g* at 4°C for 1.5 h in a Beckman Coulter 70.1 Ti Rotor. Samples were fractionated into 16 samples of unequal volume. Top fractions contained minimal cellular components, bottom fractions contained concentrated bands of cellular organelles and were separated into smaller fraction volumes.

Confocal imaging

All images were taken using a Leica (TCS SP5) confocal microscope. Lamp1 antibody was from the Iowa Hybridoma Bank.

Data analysis

Data are presented as the mean ± standard error of the mean (SEM). Statistical comparisons were made using analysis of variance (ANOVA). A P value < 0.05 was considered statistically significant.

Supplementary Material

Refer to Web version on PubMed Central for supplementary material.

Acknowledgments

This work was supported by start-up funds to H.X. from the Department of MCDB and Biological Science Scholar Program, the University of Michigan, an NIH RO1 grant (NS062792 to H.X), pilot grants (to H.X.) from the UM Initiative on Rare Disease Research, Michigan Alzheimer's Disease Research Center, National Multiple Sclerosis Society, and NIH R01 GM50403 to L.S.W. We thank Amy Chang for her constant assistance/support and providing yeast strains, Patrick Masson for the pEVP11/AEQ plasmid, Dan Kilonsky for pCuGFP416 vector, Rob Botelho for Fab1 strains, Dr. Pietro De Camili for CFP-FRB-MTM1 and CFP-FKBP*2-Rab5 constructs, Dr.Banasfe Larijani for RFP-FRB-MTM1 and EGFP-FKBP*2-Rab5 constructs, Dr. Martha Cyert for Yvc1-GFP construct, and David Ginsburg's lab for the electroporator. We are grateful to S. Park, S. Punthambaker, S. Liu, and C. Li for assistance, and L. Yue, D. Ren, and M. Meisler for comments on an earlier version of the manuscript. We appreciate the encouragement and helpful comments from other members of the Xu laboratory.

References

1. Hay JC. Calcium: a fundamental regulator of intracellular membrane fusion? EMBO reports 2007;8:236–240. [PubMed: 17330068]
2. Peters C, Mayer A. Ca^{2+}/calmodulin signals the completion of docking and triggers a late step of vacuole fusion. Nature 1998;396:575–580. [PubMed: 9859992]
3. Luzio JP, Pryor PR, Bright NA. Lysosomes: fusion and function. Nature reviews 2007;8:622–632.
4. Dong XP, Wang X, Xu H. TRP channels of intracellular membranes. Journal of neurochemistry 2010;113:313–328. [PubMed: 20132470]
5. Cheng X, Shen D, Samie M, Xu H. Mucolipins: Intracellular TRPML1-3 channels. FEBS letters. 2010
6. Puertollano R, Kiselyov K. TRPMLs: in sickness and in health. American Journal of physiology 2009;296:F1245–F1254. [PubMed: 19158345]
7. Sun M, et al. Mucolipidosis type IV is caused by mutations in a gene encoding a novel transient receptor potential channel. Human molecular genetics 2000;9:2471–2478. [PubMed: 11030752]
8. Nilius B, Owsianik G, Voets T, Peters JA. Transient receptor potential cation channels in disease. Physiological reviews 2007;87:165–217. [PubMed: 17237345]
9. Bonangelino CJ, et al. Osmotic stress-induced increase of phosphatidylinositol 3,5-bisphosphate requires Vac14p, an activator of the lipid kinase Fab1p. Journal of cell biology 2002;156:1015–1028. [PubMed: 11889142]
10. Chow CY, et al. Mutation of FIG4 causes neurodegeneration in the pale tremor mouse and patients with CMT4J. Nature 2007;448:68–72. [PubMed: 17572665]
11. Dove SK, Dong K, Kobayashi T, Williams FK, Michell RH. Phosphatidylinositol 3,5-bisphosphate and Fab1p/PIKfyve underPPIn endo-lysosome function. The Biochemical journal 2009;419:1–13. [PubMed: 19272020]
12. Zhang Y, et al. Loss of Vac14, a regulator of the signaling lipid phosphatidylinositol 3,5-bisphosphate, results in neurodegeneration in mice. Proceedings of the National Academy of Sciences of the United States of America 2007;104:17518–17523. [PubMed: 17956977]
13. Duex JE, Nau JJ, Kauffman EJ, Weisman LS. Phosphoinositide 5-phosphatase Fig 4p is required for both acute rise and subsequent fall in stress-induced phosphatidylinositol 3,5-bisphosphate levels. Eukaryot Cell 2006;5:723–731. [PubMed: 16607019]
14. Botelho RJ, Efe JA, Teis D, Emr SD. Assembly of a Fab1 phosphoinositide kinase signaling complex requires the Fig4 phosphoinositide phosphatase. Molecular biology of the cell 2008;19:4273–4286. [PubMed: 18653468]
15. Poccia D, Larijani B. Phosphatidylinositol metabolism and membrane fusion. The Biochemical journal 2009;418:233–246. [PubMed: 19196244]
16. Jin N, et al. VAC14 nucleates a protein complex essential for the acute interconversion of PI3P and $PI(3,5)P_2$ in yeast and mouse. EMBO 2008;27:3221–3234.
17. Shen J, et al. Deficiency of MIP/MTMR14 phosphatase induces a muscle disorder by disrupting Ca^{2+} homeostasis. Nature cell biology 2009;11:769–776.
18. Chow CY, et al. Deleterious variants of FIG4, a phosphoinositide phosphatase, in patients with ALS. The American jounral of human genetics 2009;84:85–88.
19. Pryor PR, Reimann F, Gribble FM, Luzio JP. Mucolipin-1 is a lysosomal membrane protein required for intracellular lactosylceramide traffic. Traffic (Copenhagen, Denmark) 2006;7:1388–1398.
20. Dong XP, et al. Activating mutations of the TRPML1 channel revealed by proline-scanning mutagenesis. The Journal of biological chemistry 2009;284:32040–32052. [PubMed: 19638346]
21. Dong XP, et al. The type IV mucolipidosis-associated protein TRPML1 is an endolysosomal iron release channel. Nature 2008;455:992–996. [PubMed: 18794901]
22. Cooke FT, et al. The stress-activated phosphatidylinositol 3-phosphate 5-kinase Fab1p is essential for vacuole function in S. cerevisiae. Current biology 1998;8:1219–1222. [PubMed: 9811604]
23. Gary JD, Wurmser AE, Bonangelino CJ, Weisman LS, Emr SD. Fab1p is essential for PtdIns(3)P 5-kinase activity and the maintenance of vacuolar size and membrane homeostasis. Journal of cell biology 1998;143:65–79. the. [PubMed: 9763421]

24. Rudge SA, Anderson DM, Emr SD. Vacuole size control: regulation of PtdIns(3,5)P_2 levels by the vacuole-associated Vac14-Fig4 complex, a PtdIns(3,5)P_2-specific phosphatase. Molecular biology of cell 2004;15:24–36.
25. Zeevi DA, Frumkin A, Offen-Glasner V, Kogot-Levin A, Bach G. A potentially dynamic lysosomal role for the endogenous TRPML proteins. The Journal of pathology 2009;219:153–162. [PubMed: 19557826]
26. Nilius B, Owsianik G, Voets T. Transient receptor potential channels meet phosphoinositides. EMBO 2008;27:2809–2816.
27. Suh BC, Hille B. PIP2 is a necessary cofactor for ion channel function: how and why? Annu. Rev. Biophys 2008;37:175–195. [PubMed: 18573078]
28. Zoncu R, et al. A phosphoinositide switch controls the maturation and signaling properties of APPL endosomes. Cell 2009;136:1110–1121. [PubMed: 19303853]
29. Kwon Y, Hofmann T, Montell C. Integration of phosphoinositide- and calmodulin-mediated regulation of TRPC6. Molecular cell 2007;25:491–503. [PubMed: 17317623]
30. Grimm C, et al. A helix-breaking mutation in TRPML3 leads to constitutive activity underlying deafness in the varitint-waddler mouse. Proceedings of the National Academy of Sciences of the United States of America 2007;104:19583–19588. [PubMed: 18048323]
31. Xu H, Delling M, Li L, Dong X, Clapham DE. Activating mutation in a mucolipin transient receptor potential channel leads to melanocyte loss in varitint-waddler mice. Proceedings of the National Academy of Sciences of the United States of America 2007;104:18321–18326. [PubMed: 17989217]
32. Calcraft PJ, et al. NAADP mobilizes calcium from acidic organelles through two-pore channels. Nature 2009;459:596–600. [PubMed: 19387438]
33. Denis V, Cyert MS. Internal Ca^{2+} release in yeast is triggered by hypertonic shock and mediated by a TRP channel homologue. The Journal of cell biology 2002;156:29–34. [PubMed: 11781332]
34. Duex JE, Tang F, Weisman LS. The Vac14p-Fig4p complex acts independently of Vac7p and couples $PI(3,5P)_2$ synthesis and turnover. The Journal of cell biology 2006;172:693–704. [PubMed: 16492811]
35. Baars TL, Petri S, Peters C, Mayer A. Role of the V-ATPase in regulation of the vacuolar fission-fusion equilibrium. Molecular biology of the cell 2007;18:3873–3882. [PubMed: 17652457]
36. Palmer CP, et al. A TRP homolog in Saccharomyces cerevisiae forms an intracellular Ca^{2+}-permeable channel in the yeast vacuolar membrane. Proceedings of the National Academy of Sciences of the United States of America 2001;98:7801–7805. [PubMed: 11427713]
37. Chen CS, Bach G, Pagano RE. Abnormal transport along the lysosomal pathway in mucolipidosis, type IV disease. Proceedings of the National Academy of Sciences of the United States of America 1998;95:6373–6378. [PubMed: 9600972]
38. Thompson EG, Schaheen L, Dang H, Fares H. Lysosomal trafficking functions of mucolipin-1 in murine macrophages. BMC cell biology 2007;8:54. [PubMed: 18154673]
39. Treusch S, et al. Caenorhabditis elegans functional orthologue of human protein h-mucolipin-1 is required for lysosome biogenesis. Proceedings of the National Academy of Sciences of the United States of America 2004;101:4483–4488. [PubMed: 15070744]
40. Ferguson CJ, Lenk GM, Meisler MH. Defective autophagy in neurons and astrocytes from mice deficient in PI(3,5)P_2. Human molecular genetics 2009;18:4868–4878. [PubMed: 19793721]
41. Vergarajauregui S, Martina JA, Puertollano R. Identification of the penta-EF-hand protein ALG-2 as a Ca^{2+}-dependent interactor of mucolipin-1. The Journal of biological chemistry 2009;284:36357–36366. [PubMed: 19864416]
42. Roth MG. Phosphoinositides in constitutive membrane traffic. Physiological reviews 2004;84:699–730. [PubMed: 15269334]
43. Zhu MX, Ma J, Parrington J, Galione A, Mark Evans A. TPCs: Endolysosomal channels for Ca^{2+} mobilization from acidic organelles triggered by NAADP. FEBS letters. 2010
44. Huynh C, Andrews NW. The small chemical vacuolin-1 alters the morphology of lysosomes without inhibiting Ca^{2+}-regulated exocytosis. EMBO reports 2005;6:843–847. [PubMed: 16113649]
45. Kim HJ, Soyombo AA, Tjon-Kon-Sang S, So I, Muallem S. The Ca^{2+} channel TRPML3 regulates membrane trafficking and autophagy. Traffic (Copenhagen, Denmark) 2009;10:1157–1167.

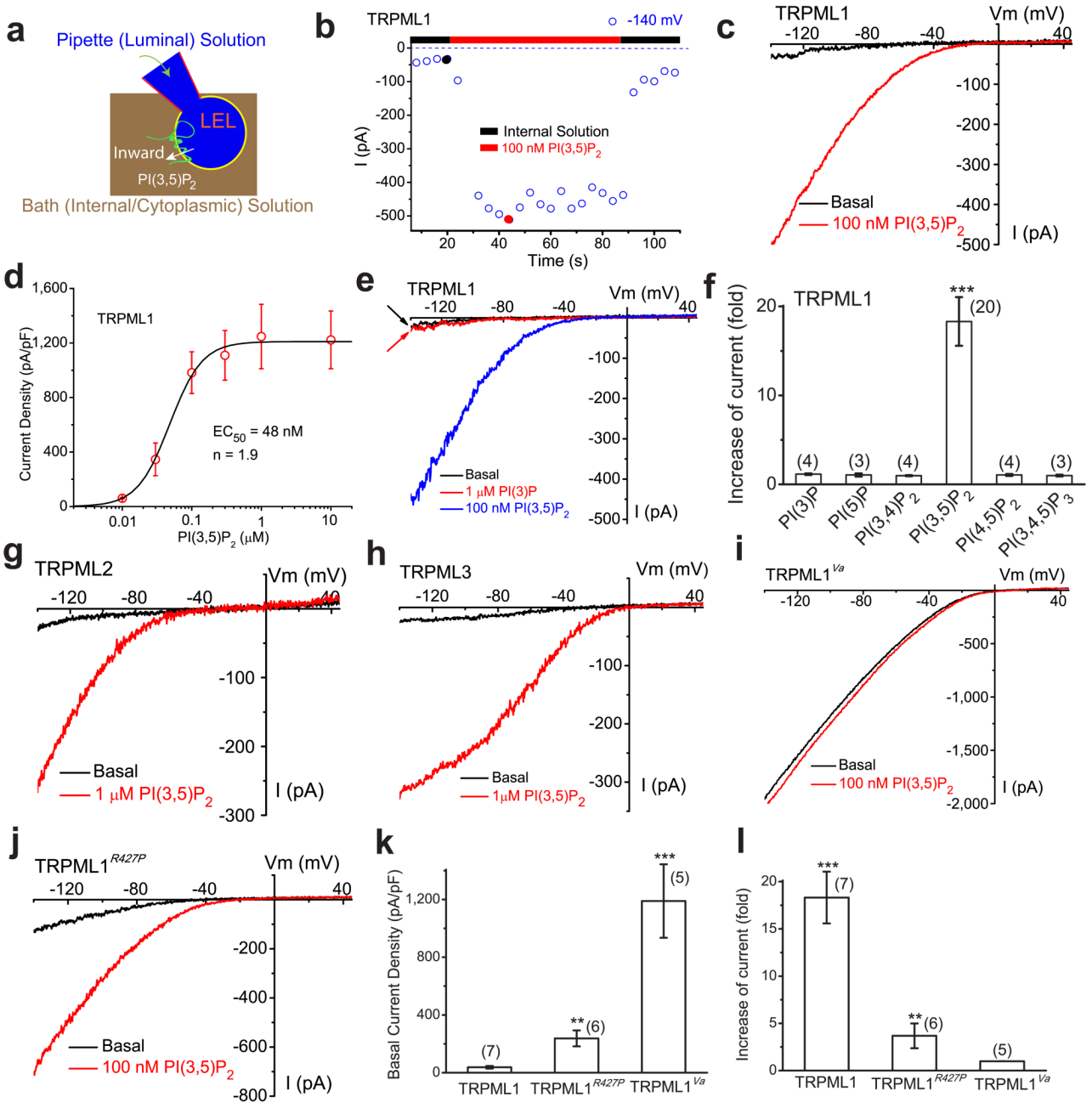

Figure 1. PI(3,5)P_2 activates recombinant TRPML channels in the endolysosomal membranes

a) Illustration of a whole-endolysosome recording configuration. Pipette (luminal) solution was a standard external (Tyrode's) solution adjusted to pH 4.6 to mimic the acidic environment of the lysosome lumen. Bath (internal/cytoplasmic) solution was a K^+-based solution (140 mM K^+-gluconate). Putative membrane topology of TRPML channels is illustrated in the late endosome and lysosome (LEL). Note that the inward current indicates cations flowing out of the endolysosome (see red arrow for the direction). **b)** Bath application of PI(3,5)P_2 (diC8, 100 nM) activated inwardly rectifying whole-endolysosome TRPML1-mediated current (I_{TRPML1}) in an enlarged endolysosome/vacuole from a TRPML1-EGFP-expressing Cos-1 cell that was pre-treated with vacuolin-1. I_{TRPML1} was elicited by repeated voltage ramps (−140

to +140 mV; 400 ms) with a 4-s interval between ramps. I_{TRPML1} exhibited a small basal current prior to $PI(3,5)P_2$ application; bath application of $PI(3,5)P_2$ to the cytoplasmic side of the endolysosome resulted in maximal activation of 18-fold of baseline within a minute, measured at −140 mV of I_{TRPML1}. **c)** Representative traces of I_{TRPML1} before (black) and after (red) $PI(3,5)P_2$ at two time points, as shown in **a** (black and red circles). Only a portion of the voltage protocol is shown; holding potential = 0 mV. **d)** Dose-dependence of $PI(3,5)P_2$-dependent activation (EC_{50} = 48 nM, n = 1.9). **e)** PI(3)P (1 μM) failed to activate I_{TRPML1}. **f**) Specific activation of TRPML1 by $PI(3,5)P_2$ (in 100 nM), but not other diC8 PIPs (all in 1 μM). **g**) Activation of whole-endolysosome I_{TRPML2} by $PI(3,5)P_2$ (1 μM). **h**) Activation of whole-endolysosome I_{TRPML3} by $PI(3,5)P_2$ (1 μM). **i**) Whole-endolysosome $I_{TRPML1\text{-}Va}$ exhibited high basal activity but was insensitive to $PI(3,5)P_2$ (100 nM). **j)** Whole-endolysosome $I_{TRPML1\text{-}R427P}$ was weakly activated by $PI(3,5)P_2$. **k)** Basal current amplitudes of whole-endolysosome I_{TRPML1}, $I_{TRPML1\text{-}R427P}$, and $I_{TRPML1\text{-}Va}$. **l)** Effects of $PI(3,5)P_2$ on I_{TRPML1}, $I_{TRPML1\text{-}R427P}$, and $I_{TRPML1\text{-}Va}$. For histogram graphs of all figures including panels (**f, k, l**) of this figure, data are presented as the mean ± standard error of the mean (SEM); the n numbers are in parentheses. Statistical comparisons were made using analysis of variance (ANOVA): *P* value < 0.05 was considered statistically significant and indicated with asterisks (*, 0.01< $P < 0.05$; **, $P < 0.01$; ***, $P < 0.001$).

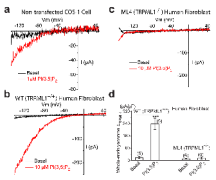

Figure 2. PI(3,5)P_2 activates endogenous TRPML-like currents in the endolysosomal membranes

a) An endogenous inwardly rectifying TRPML-like current ($I_{TRPML1\text{-}L}$) activated by PI(3,5)P_2 (10 μM) in a vacuole isolated from a non-transfected Cos-1 cell. **b**) Large PI(3,5)P_2-activated $I_{TRPML1\text{-}L}$ in a vacuole isolated from wild type (WT) human skin fibroblast cell. **c**) Lack of significant PI(3,5)P_2-activated $I_{TRPML1\text{-}L}$ in a vacuole isolated from a human ML4 (TRPML1$^{-/-}$) skin fibroblast cell. **d**) Endogenous PI(3,5)P_2-activated $I_{TRPML\text{-}L}$ in WT and TRPML1$^{-/-}$ human fibroblasts. For statistical analysis: ***, $P < 0.001$; NS (non-significant), $P > 0.05$).

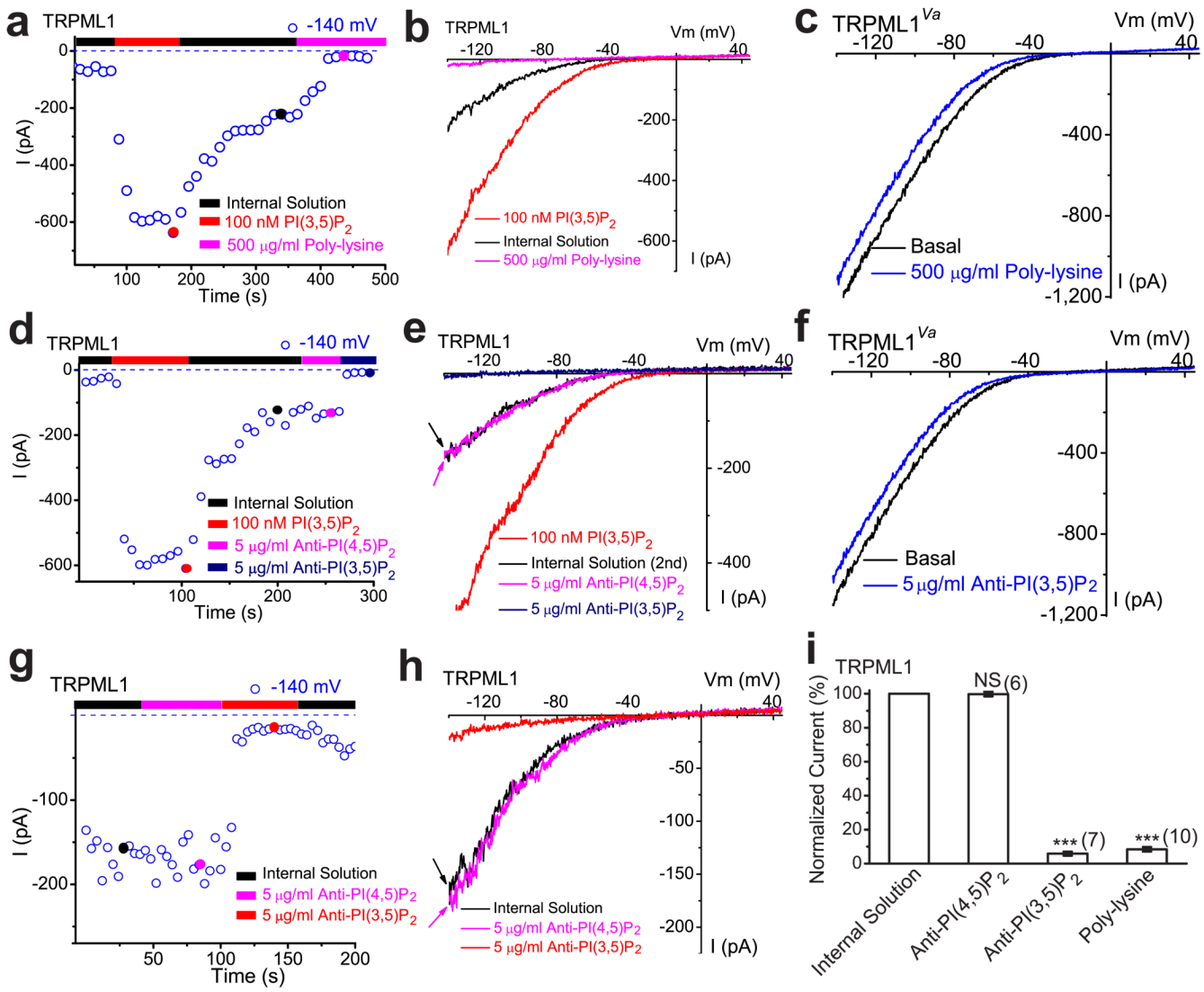

Figure 3. A decrease in PI(3,5)P_2 by chelating agents suppresses TRPML1 channel activity in the endolysosomal membrane

a) Post- PI(3,5)P_2 quasi-steady state I_{TRPML1} was inhibited by bath (internal/cytoplasmic) application of poly-lysine (500 μg/ml) to an enlarged endolysosome from a TRPML1-EGFP-expressing Cos-1 cell. I_{TRPML1} increased with addition of 100 nM PI(3,5)P_2, but gradually reduced to a quasi-steady state level upon washout. **b)** Representative traces of I_{TRPML1} at three time points, as shown in **a**: upon PI(3,5)P_2 application (red), washout (black), and poly-lysine application (magenta). **c**) Lack of poly-lysine (500 μg/ml) effect on whole-endolysosome $I_{TRPML1\text{-}Va}$. **d)** Post- PI(3,5)P_2 quasi-steady state I_{TRPML1} was inhibited by bath application of neutralizing anti-PI(3,5)P_2(5 μg/ml), but not anti-PI(4,5)P_2 (5 μg/ml). **e)** Representative traces of I_{TRPML1} at three time points, as shown in **d. f)** Lack of anti- PI(3,5) P_2 (5 μg/ml) effect on whole-endolysosome $I_{TRPML1\text{-}Va}$. **g, h)** Large basal pre- PI(3,5)P_2 I_{TRPML1} was inhibited by bath application of neutralizing anti-PI(3,5)P_2 (5 μg/ml), but not anti-PI(4,5)P_2. **i)** I_{TRPML1} was inhibited by more than 90% by bath (internal/cytoplasmic) application of poly-lysine (500 μg/ml) or PI(3,5)P_2 antibody.

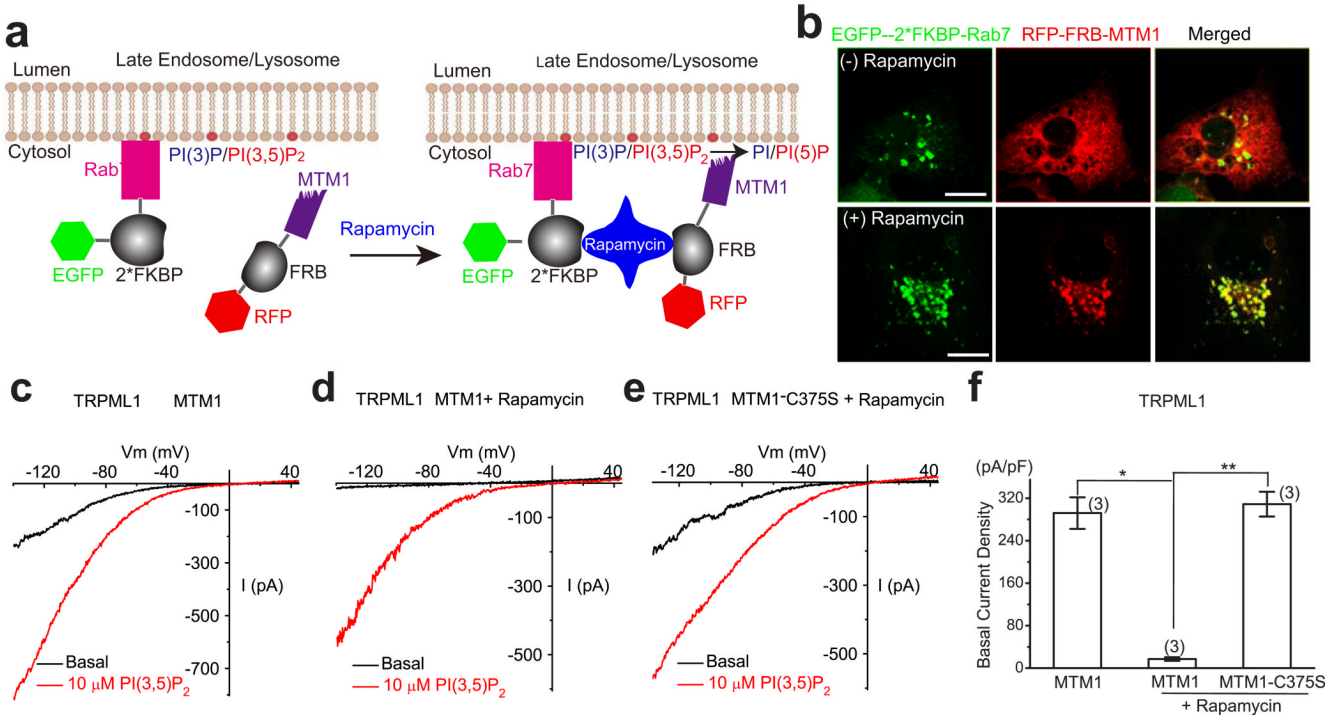

Figure 4. A decrease in PI(3,5)P_2 level by a translocatable lipid phosphatase suppresses TRPML1 channel activity in the endolysosomal membrane

a) Recruitment of MTM1 to endolysosomal membranes by rapamycin-dependent heterodimerization of RFP-FRB-MTM1 and EGFP-2*FKBP-Rab7. Rab7 is a LEL-specific Rab protein. MTM1 is a PI-3 phosphatase that can convert PI(3,5)P_2 and PI(3)P into PI(5)P and PI, respectively. **b)** Rapamycin-dependent heterodimerization of RFP-FRB-MTM1 and EGFP-2*FKBP-Rab7 alters subcellular localization of MTM1. Cos-1 cells were transfected with both RFP-FRB-MTM1 and EGFP-2*FKBP-Rab7. Rapamycin (500 nM; 20 min) treatment promotes co-localization of MTM1-RFP with Rab7-EGFP. Scale Bar = 10 μm. **c-f)** The effects of MTM1 on I_{TRPML1}. Cos-1 cells were co-transfected with human TRPML1-myc, RFP-FRB-MTM1 or RFP-FRB-MTM1-C375S, and EGFP-2*FKBP-Rab7. MTM1 was recruited to LEL membranes by rapamycin (500 nM) -dependent heterodimerization of RFP-FRB-MTM1 and EGFP-2*FKBP-Rab7. **c)** I_{TRPML1} in MTM1-transfected cells before rapamycin treatment. **d)** I_{TRPML1} in MTM1-transfected cells after rapamycin treatment. **e)** I_{TRPML1} in MTM1-C357S-transfected cells after rapamycin treatment. **f)** Differential effects of WT and inactive mutant (C375S) MTM1 on basal whole-endolysosome I_{TRPML1} For statistical analysis: *, $0.01 < P < 0.05$; **, $P < 0.01$).

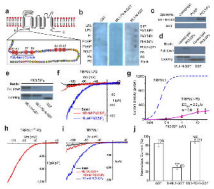

Figure 5. Direct binding of PI(3,5)P_2 to the TRPML1 N-terminus requires multiple positively-charged amino acid residues

a) The cytoplasmic N-terminus of TRPML1 contains a poly-basic region and clusters of positively charged amino acid residues as potential PI(3,5)P_2 binding sites. The positively charged amino acid residues (Arg and Lys) that were mutated into neutral amino acids Gln (Q) in this study are shown with enlarged circles and their amino acid residue numbers. **b)** Protein-lipid overlays. The strip contained 15 different types of lipids: PA, phosphatidic acid; S1P, sphingosine-1-phosphate. Three purified proteins were used to probe the strip: GST alone (left panel), GST-fused to the N-terminal fragment of TRPML1 (ML1-N-GST; right panel), and Gln-substituted mutant of ML1-N-GST (ML1-7Q-N-GST; middle). Proteins were detected with anti-GST antibodies. **c)** Liposome pull-down assay. Liposomes were incubated with purified GST-fusion proteins, centrifuged, and associated proteins visualized by Western blot with GST antibodies. **d)** Binding of GST-ML1-N to agarose beads conjugated to PI(3,5)P_2, but not control lipids; GST alone failed to pull down PI(3,5)P_2-conjugated beads. **e)** Compared to GST-ML1-N, GST-ML1-7Q-N exhibited significantly weaker binding to PI(3,5)P_2-conjugated agarose beads. **f)** Whole-endolysosome $I_{TRPML1\text{-}7Q}$ was weakly activated by high concentrations of PI(3,5)P_2. **g)** PI(3,5)P_2 dose dependence of $I_{TRPML1\text{-}7Q}$. Dotted line indicates the dose dependence of I_{TRPML1} (repotted from Fig. 1d). **h)** Large basal whole-endolysosome $I_{TRPML1\text{-}Va\text{-}7Q}$. Charge-removing Gln substitutions (7Q) were introduced into the gain-of-function *Va* background. **i)** GST-ML1-N peptide (5 μg/ml) reduced PI(3,5)P_2-dependent activation of whole-endolysosome I_{TRPML1}.. **j)** Charge-removing Gln-substituted substitutions (7Q) abolished the inhibitory effect of GST-ML1-N peptide.

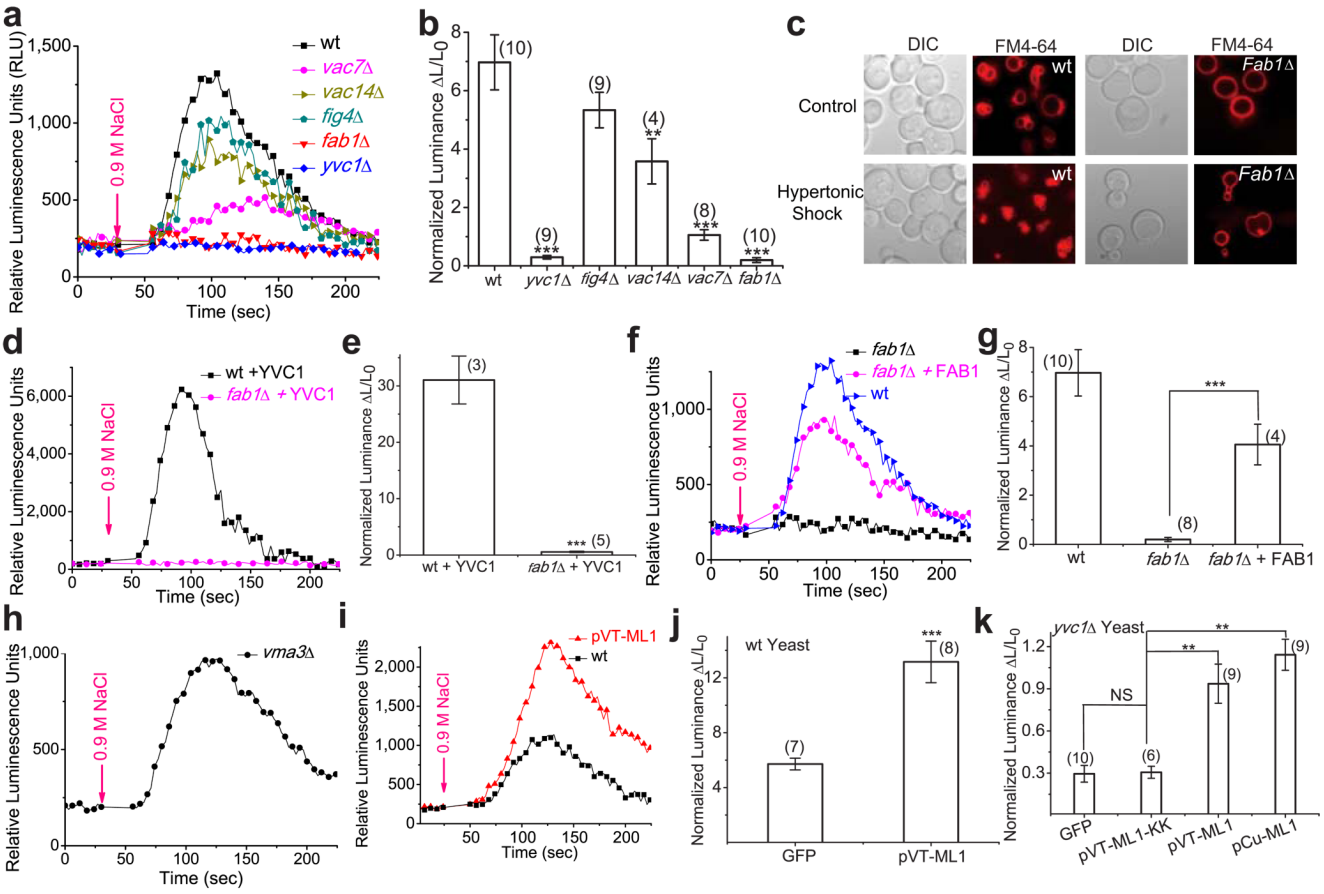

Figure 6. Ca^{2+} release from yeast vacuoles after hyperosmostic shock is dependent on $PI(3,5)P_2$ production

a) Representative Ca^{2+} response measured with aequorin-mediated luminescence in wild-type (wt), *yvc1Δ*, and $PI(3, 5P)_2$-deficient strains (*vac7Δ*, *vac14Δ*, *fig4Δ*, *fab1Δ*) upon hyperosmotic shock induced by addition of 0.9 M NaCl. **b)** Quantitative data to show luminescence responses upon hyperosmotic shock in different yeast strains. Fold-response was normalized to basal luminescence prior to shock. **c)** Hyperosmotic shock increases the number of vacuoles and decreases the vacuolar volume in wild type, but not fab1 mutant yeast strains. Both WT and *fab1Δ* cells were labeled with FM4-64 dye to visualize vacuole volume and the number of vacuole lobes. Cells were treated with 0.45M NaCl and viewed by fluorescence microscopy. **d, e)** Overexpression of YVC1 in *fab1Δ* cells failed to restore hyperosmolarity-induced Ca^{2+} response. **f, g)** Overexpression of *FAB1* in *fab1Δ* cells restored hyperosmolarity-induced Ca^{2+} response. **h, i)** Overexpression of TRPML1 in WT yeast cells increased hyperosmolarity-induced Ca^{2+} response. **j)** Hyperosmotic shock induces vacuolar Ca^{2+} release in *vma3* mutant yeast strains. **k)** Overexpression of TRPML1, but not pore mutant TRPML1-KK (in pCu and pVT expression vectors), in *yvc1Δ* yeast cells resulted in small but significant hyperosmolarity-induced Ca^{2+} response.

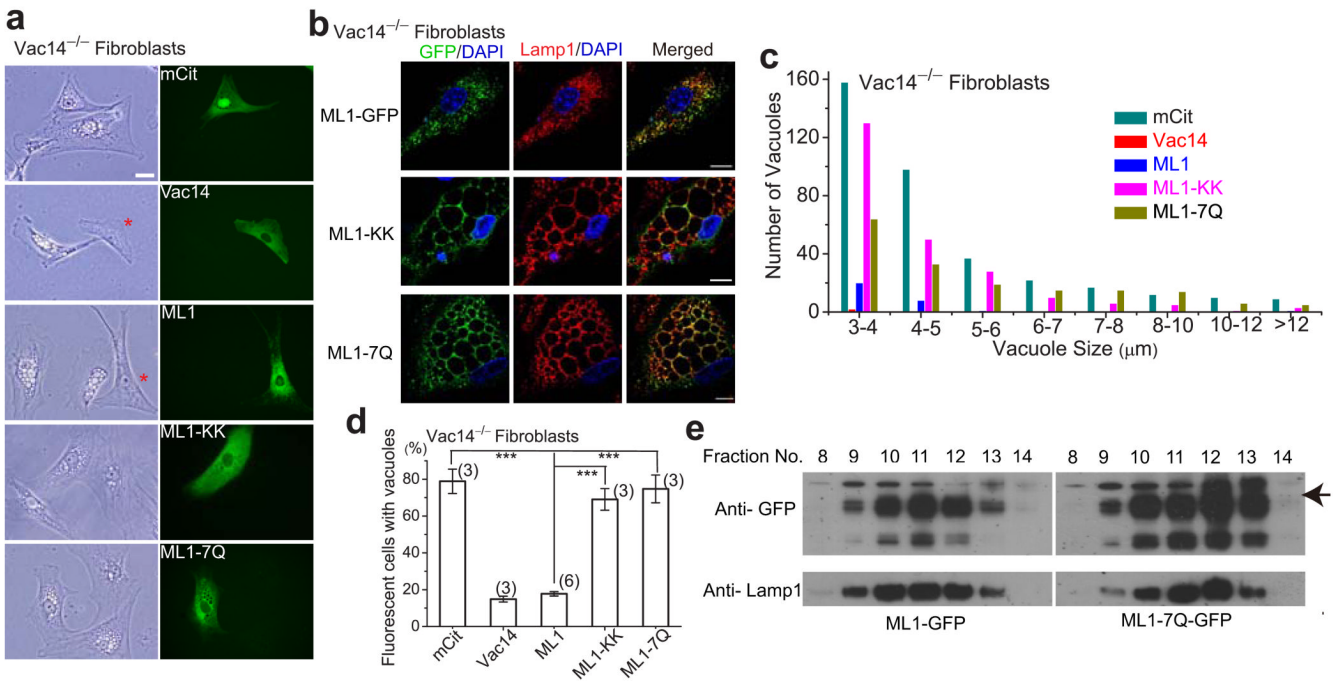

Figure 7. Overexpression of TRPML1 rescues the enlarged endolysosome phenotype of PI(3,5)P_2-deficient mouse fibroblasts

a, b) The effects of overexpression of WT TRPML1 and pore (ML1-KK) or PI(3,5)P_2-insensitive (ML1-7Q) mutant TRPML1 on the number and size of the vacuoles in Vac14$^{-/-}$ fibroblasts. Cultured Vac14$^{-/-}$ mouse fibroblast cells exhibited variable numbers (1–20) of large (> 3 μm) vacuoles/endolysosomes. Non-vacuolated cells are indicated with asterisk. Scale Bar = 20 μm. **b)** TRPML1, ML1-KK, and ML1-7Q proteins were co-localized in Lamp1-positive compartments of Vac14$^{-/-}$ fibroblast cells. **c)** Large vacuoles in 75% of vector (mCit) -transfected Vac14$^{-/-}$ fibroblast cells. Overexpression of Vac14-mCit or EGFP-ML1 reduced the percentage (of enlarged vacuoles) to approximately 15%, while the 75% of EGFP-ML1-KK or EGFP-ML1-7Q-transfected cells contained enlarged vacuoles. **d)** Histogram analysis of the vacuole size/number in Vac14$^{-/-}$ fibroblasts transfected with indicated constructs. **e)** Fractionation analysis reveals co-localization of TRPML1 and TRPML1-7Q with Lamp-1. Gradient cellular fractionations were obtained using ultracentrifugation. Both TRPML1 and TRPML1-7Q proteins were concentrated in Lamp1-rich fractionations.

Table 1

Yeast strains.

Genotype	Strains	Genetic background	References
WT	LWY7217	MATa leu2,3–112 ura3-52 his3-Δ200 trp1-Δ901 lys2-Δ801 suc2-Δ9	Ref. 34
*vac7*Δ	LWY2054	LWY 7217; vac7Δ::HIS3	Ref. 34
WT	LWY 7235	MATa leu2,3–112 ura3-52 his3-Δ200 trp1-Δ901 lys2-Δ801 suc2-Δ9	Ref. 34
*vac14*Δ	LWY 5177	LWY 7235; vac14Δ::TRP1	Ref. 34
*fig4*Δ	LWY 6474	LWY 7235; fig4Δ::TRP1	Ref. 34
*yvc1*Δ	LWY 6848	LWY 7235; yvc1Δ::Kan	This study
WT	SEY6210	MATa leu2-3,112 ura3-52 his3-Δ200 trp1-Δ901 lys2-Δ801 suc2-Δ9	Ref. 14
*fab1*Δ	fab1Δ2	SEY6210; fab1Δ::HIS3	Ref. 14
*vma3*Δ	Vma3Δ	MATa his3-Δ1 leu2Δ0, Met15Δ0 ura3Δ0 vmaΔ:: Kan MX	Open Biosystems